

Article

The Mechanical Properties and Elastic Anisotropies of Cubic Ni₃Al from First Principles Calculations

Xinghe Luan ^{1,2}, Hongbo Qin ^{1,2,*} , Fengmei Liu ^{1,*}, Zongbei Dai ¹, Yaoyong Yi ¹ and Qi Li ¹

¹ Guangdong Provincial Key Laboratory of Advanced Welding Technology, Guangdong Welding Institute (China-Ukraine E.O. Paton Institute of Welding), Guangzhou 541630, China; 1601201040@mails.guet.edu.cn (X.L.); dai_zongbei@163.com (Z.D.); yiyy@gwi.gd.cn (Y.Y.); liq@gwi.gd.cn (Q.L.)

² Key Laboratory of Guangxi Manufacturing System and Advanced Manufacturing Technology, Guilin University of Electronic Technology, Guilin 541004, China

* Correspondence: qinhb@guet.edu.cn (H.Q.); liufm@gwi.gd.cn (F.L.)

Received: 21 June 2018; Accepted: 22 July 2018; Published: 25 July 2018



Abstract: Ni₃Al-based superalloys have excellent mechanical properties which have been widely used in civilian and military fields. In this study, the mechanical properties of the face-centred cubic structure Ni₃Al were investigated by a first principles study based on density functional theory (DFT), and the generalized gradient approximation (GGA) was used as the exchange-correlation function. The bulk modulus, Young's modulus, shear modulus and Poisson's ratio of Ni₃Al polycrystal were calculated by Voigt-Reuss approximation method, which are in good agreement with the existing experimental values. Moreover, directional dependences of bulk modulus, Young's modulus, shear modulus and Poisson's ratio of Ni₃Al single crystal were explored. In addition, the thermodynamic properties (e.g., Debye temperature) of Ni₃Al were investigated based on the calculated elastic constants, indicating an improved accuracy in this study, verified with a small deviation from the previous experimental value.

Keywords: intermetallic compound; Ni₃Al single crystal; first principles; mechanical property; elastic anisotropy

1. Introduction

Ni-Al alloys, especially Ni-Al single crystal alloys, have been widely applied as structural materials and functional materials in civilian and military fields, due to their high strength, high temperature stability, corrosion and oxidation resistances in aggressive environments [1–5]. As the most promising and valued Ni-Al alloys, L1₂-ordered Ni₃Al-based single crystal alloys are well known as superalloys because of their excellent mechanical properties at high temperature [6], which have been extensively used for the hot components of gas turbines [7]. Ni₃Al is a kind of intermetallic compound, and its elastic modulus, bulk modulus, shear modulus have been explored by experimental methods. It should be noted that, due to the variation of material preparation, processing and test methods, the mechanical properties of Ni₃Al measured by experimental methods are discrete. For example, the bulk modulus of L1₂-ordered Ni₃Al explored by Pearson et al. is 229.2 GPa [8] while the value obtained by Yasuda et al. is 171.0 GPa [9]. In order to break through the limitation derived from experimental methods, in recent years, first principles calculations have been successfully conducted to calculate the elastic properties of alloys and intermetallics [10–14]. Based on first principles, Wen et al. [1] calculated the bulk modulus and Young's modulus of Ni₃Al, as well as the effects of pressure on the mechanical properties. Kim et al. [15] investigated the mechanical parameters of Ni₃Al, such as bulk modulus, Young's modulus, shear modulus, and the influences of several typical

doped alloying elements on them. Huang et al. [16] computed various elastic moduli and elastic constants of Ni₃Al via first principles and pointed out these values coincide well with other theoretical and experimental results. In addition, Wen et al. [2] investigated the behaviour of Ni₃Al by calculating the stress-strain curve and the corresponding mechanical stability. Ni₃Al-based alloys have been largely applied as single crystal materials [17–19], while most of the previous studies based on experiments and first principles calculations neglect the anisotropic behaviour of Ni₃Al single crystal, which has great influences on the abnormal crystal grains growth, microstructure transformation/formation, and the microcrack development [20,21]. So, it is of great significance to study the anisotropic mechanical properties for the reliability evaluation of Ni₃Al-based alloys.

Thus far, anisotropic mechanical properties of Ni₃Al single crystal alloys is not yet clear due to difficulties of accurately measuring the anisotropic mechanical properties. In the present study, the mechanical properties and elastic anisotropies, such as the anisotropy of elastic modulus, bulk modulus, shear modulus and Poisson's ratio, were investigated by first principles calculations.

2. Computational Methods and Details

The L1₂-ordered Ni₃Al compound has a face-centred cubic structure with a space group of *Pm-3m* with $a = b = c = 3.572 \text{ \AA}$ and $\alpha = \beta = \gamma = 90^\circ$, wherein the atomic locations of Ni and Al atoms in an elementary cell are 1a (0.5, 0.5, 0) and 1a (0, 0, 0), respectively, as depicted in Figure 1 [22]. In this study, the ab initio density functional theory calculation was performed using the Cambridge Sequential Total Energy Package (CASTEP) program [23]. Meanwhile, the generalized gradient approximation (GGA) [24] of the revised Perdew-Burke-Ernzerhof formalism [25] and the local density approximation (LDA) [26] proposed by Ceperley and Alder were operated to calculate the exchange-correlation potential, respectively. The Vanderbilt ultra-soft pseudopotentials [27] and Broyden Fletcher Goldfarb Shanno algorithm [28,29] were used to optimise the crystal models. The cutoff energy and *k* point were set to be 600 eV and $10 \times 10 \times 10$, respectively. The convergence tolerance of energy was set at 5.0×10^{-6} eV/atom. Meanwhile, the self-consistent field (SCF) convergence threshold was 5.0×10^{-7} eV/atom with a maximum atomic displacement of 5.0×10^{-4} Å. The maximum ionic Hellmann-Feynman force and maximum stress were less than 0.01 eV/Å and 0.02 GPa, respectively.

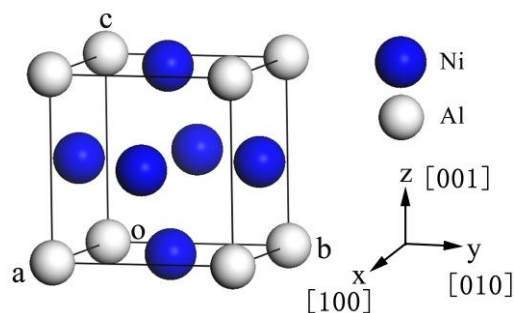


Figure 1. Crystal structure of cubic Ni₃Al.

3. Results and Discussion

3.1. Lattice Constants

The optimised lattice constants and previous experimental results are listed in Table 1 for comparison. It is conspicuous that the GGA results are in agreement with the experimental values: the maximum difference of lattice constants is merely around 0.14% and that of volumes is 0.397%, demonstrating the effectiveness of the proposed simulation model. Generally, the previous and present calculated data obtained from GGA are similar, and the difference is less than 1%. However, when using LDA, the calculated lattice volume is about 7% smaller than the experimental data, which is induced by the difference between GGA and LDA. LDA assumes that the local exchange-correlation

energy is same in a uniform electron gas with the same density, resulting in the underestimation of the exchange-correlation in regions of low electron density. Accordingly, LDA induces smaller lattice constants, larger cohesive energies and bulk modulus. GGA introduces a dependence of exchange-correlation function on the local gradient of the electron density and typically improves the underestimation of LDA in predicting lattice constants [30]. The present work and many other works [31–33] show that, compared to LDA, GGA can get a higher accuracy in predicting lattice constants and elastic properties, therefore GGA was used in the following calculations. In our research, elastic constants of Ni₃Al were obtained by linear fitting using four strains of ± 0.001 and ± 0.003 under nine strain conditions [34].

Table 1. Calculated and experimental lattice parameters of Ni₃Al.

Lattice Parameters	<i>a</i> (Å)	<i>b</i> (Å)	<i>c</i> (Å)	<i>V</i> (Å ³)	$\Delta V/V_e$, %
Present work (GGA)	3.577	3.577	3.577	45.757	+0.397
Present work (LDA)	3.486	3.486	3.486	42.377	−7.019
GGA [16]	3.569	3.569	3.569	45.461	−0.252
GGA [35]	3.561	3.561	3.561	45.156	+0.922
LDA [35]	3.486	3.486	3.486	42.363	−7.050
Experiment [22]	3.572	3.572	3.572	45.576	–

3.2. Elastic Properties

The elastic constants are essential parameters that can correlate the microscopic properties of materials with macroscopic mechanical behaviours and then provide the information of crystal stability and stiffness. The relationship between stress and strain is directly determined by Hooke's law $\sigma_{ij} = C_{ijkl}\varepsilon_{ij}$, where C_{ijkl} represents the elastic constants. If Hooke's law is applied to the lattice dynamics, combining the lattice symmetry, thus the stress-strain matrix of Ni₃Al single crystal can be written in the following form.

$$\begin{pmatrix} \sigma_1 \\ \sigma_2 \\ \sigma_3 \\ \tau_1 \\ \tau_2 \\ \tau_3 \end{pmatrix} = \begin{pmatrix} C_{11} & C_{12} & C_{13} & 0 & 0 & 0 \\ & C_{22} & C_{23} & 0 & 0 & 0 \\ & & C_{33} & 0 & 0 & 0 \\ & & & C_{44} & 0 & 0 \\ Sym. & & & & C_{55} & 0 \\ & & & & & C_{66} \end{pmatrix} \begin{pmatrix} \varepsilon_1 \\ \varepsilon_2 \\ \varepsilon_3 \\ \gamma_1 \\ \gamma_2 \\ \gamma_3 \end{pmatrix}$$

where σ_i , τ_i , ε_i , γ_i are the normal stress, shearing stress, the corresponding normal strain and shearing strain, respectively. The elastic flexibility matrix S_{ij} can be written as the inverse matrix of the elastic stiffness matrix C_{ij} , i.e., $[S_{ij}] = [C_{ij}]^{-1}$. As for cubic crystal, because of lattice symmetry, there are three independent variables in C_{ij} and S_{ij} , respectively: C_{11} , C_{12} , C_{44} and S_{11} , S_{12} , S_{44} . In this study, the elastic constants calculated based on the cubic Ni₃Al crystal structure are tabulated in Table 2, and the calculated values of S_{11} , S_{12} and S_{44} in this paper are 0.009, −0.004 and 0.008, respectively.

Table 2. Calculated and experimental elastic constants for Ni₃Al single crystal.

Elastic Constant	C_{11}	C_{12}	C_{44}
Present work	240.104	160.034	123.831
GGA [6]	225.3	157.6	121.1
GGA [36]	232.7	154.5	123.0
GGA [35]	230.31	162.51	124.79
Experiment [37]	224.3	148.6	125.8

The calculated outcomes of first principles ($C_{11} = 240.1$ GPa, $C_{12} = 160.0$ GPa, $C_{44} = 123.8$ GPa) are consistent with previous calculations and experimental values ($C_{11} = 224.3$ GPa, $C_{12} = 148.6$ GPa, $C_{44} = 125.8$ GPa). The elastic constants calculated for the cubic crystal should satisfy the following mechanical stability criteria [38]:

$$C_{11} - C_{12} > 0, C_{11} > 0, C_{44} > 0, C_{11} + 2C_{12} > 0 \quad (1)$$

By substituting the three calculated elastic constants into the above equation, we found that the present results match the above criteria obviously, indicating that Ni_3Al single crystal is an intrinsically stable system. Moreover, the bulk modulus, shear modulus and elastic modulus were calculated using the Voigt-Reuss approximation [39]. The upper limit and lower limit of the actual effective modulus correspond to Voigt bound and Reuss bound obtained by the average polycrystalline modulus based on two assumptions: uniform strain and uniform stress throughout a polycrystal, respectively [30]. For cubic lattices, Voigt bulk modulus (B_V) and shear modulus (G_V) are

$$B_V = \frac{1}{3}(C_{11} + 2C_{12}) \quad (2)$$

$$G_V = \frac{1}{5}(C_{11} - C_{12} + 3C_{44}) \quad (3)$$

and the Reuss bulk modulus (B_R) and Reuss shear modulus (G_R) are defined as

$$B_R = \frac{1}{3S_{11} + 6S_{12}} \quad (4)$$

$$G_R = \frac{15}{4S_{11} - 4S_{12} + 3S_{44}} \quad (5)$$

Voigt and Reuss equations represent upper and lower limits of the true polycrystalline constants, and the practical estimate of the bulk and shear moduli can be treated as the arithmetic mean of the two extremes [40]. The Hill's average for the shear modulus (G) and bulk modulus (B) is given by

$$B = \frac{1}{2}(B_R + B_V) \quad (6)$$

$$G = \frac{1}{2}(G_R + G_V) \quad (7)$$

while Young's modulus (E) and Poisson's ratio (ν) are given by

$$E = \frac{9BG}{3B + G} \quad (8)$$

$$\nu = \frac{3B - E}{6B} \quad (9)$$

the bulk modulus, shear modulus, Young's modulus, and Poisson's ratio calculated in this study are listed in Table 3. The results calculated in this paper are very close to previously calculated values and experimental values measured by Prikhodko et al. [41], which can effectively verify the reliability of the calculation results. In addition, either the ductility or the brittleness of metallic material can affect the mechanical properties directly, and determine the failure mode. Pugh et al. [42] introduced the ratio of bulk modulus to shear modulus B/G as a reference for the judgments of the ductility of a material. If the value of B/G is large, it means that the material has a good ductility, otherwise it will be characterised by prominent brittleness. For a normal material, if its B/G value exceeds 1.75, indicating it is a ductile material, otherwise it is brittle [30]. According to the data given in Table 3, the B/G value of Ni_3Al alloy is 2.368, which is obviously higher than the critical value 1.75, demonstrating that Ni_3Al is a ductile material which agrees with the experimental result reported in a previous study [43].

Further, the Vicker's hardness H_V is another important mechanical property of materials, which can be predicted by Equation (10) [44].

$$H_V = 0.92(B/G)^{1.3137} G^{0.708} \quad (10)$$

It is reported that materials with Vickers hardness larger than 40 GPa can be classified as superhard materials [45]. For the calculated value of H_V of Ni_3Al is 54.004 GPa, it is supposed that Ni_3Al and Ni_3Al -based materials have an excellent ability to resist being scratched or dented.

Table 3. Calculated elastic properties of Ni_3Al .

	B_V , GPa	B_R , GPa	G_V , GPa	G_R , GPa	B , GPa	G , GPa	E , GPa	ν	B/G	H_V
Present Work	186.724	186.724	90.313	67.401	186.724	78.857	207.378	0.315	2.368	54.004
GGA [6]	–	–	–	–	180.2	72.9	–	–	–	–
GGA [36]	–	–	–	–	180.6	77.8	204.0	–	–	–
GGA [35]	–	–	–	–	184.49	73.05	196.65	0.320	–	–
Exp. [41]	–	–	–	–	173.9	77.8	203.1	0.305	2.235	–

3.3. Elastic Anisotropy

The elastic anisotropy can be described by the universal anisotropic index A^U [46] and the percent anisotropy indexes of compression and shear (A_B and A_G) [47,48], respectively. The calculation formulas are expressed as follows

$$A^U = 5 \frac{G_V}{G_R} + \frac{B_V}{B_R} - 6 \quad (11)$$

$$A_B = \frac{B_V - B_R}{B_V + B_R} \quad (12)$$

$$A_G = \frac{G_V - G_R}{G_V + G_R} \quad (13)$$

for the three indexes, the value of zero indicates elastic isotropy while the variation from zero means anisotropic elastic properties. After calculation, it is found that the A^U value of Ni_3Al is 1.670, indicating that Ni_3Al exhibits anisotropic behaviour. The value 0.000 for A_B indicates the isotropic compression of Ni_3Al , while the A_G value of 0.145 shows that Ni_3Al exhibits shear anisotropy. As a measure of the anisotropy degree for the bondings between atoms in different crystal planes, the shear anisotropic factors are used. The shear anisotropic factor A_1 for {100} planes is written as [48]

$$A_1 = \frac{4C_{44}}{C_{22} + C_{33} - 2C_{13}} \quad (14)$$

shear anisotropic factors A_2 and A_3 for the {010} and {001} planes are given as Equations (15) and (16), respectively,

$$A_2 = \frac{4C_{55}}{C_{33} + C_{11} - 2C_{23}} \quad (15)$$

$$A_3 = \frac{4C_{66}}{C_{11} + C_{22} - 2C_{12}} \quad (16)$$

For the case of isotropic crystals, the value of shear anisotropic factor is 1, and the anisotropy is reflected in the deviation from 1 [30]. In this calculation, the three values are all 3.093 (see Table 4), indicating that the Ni_3Al crystals exhibit shear anisotropy in the {100}, {010} and {001} planes evidently. In addition, the anisotropic indexes of the bulk modulus along the a axis and c axis with respect to the b axis can be written as Equations (17) and (18) [48], respectively.

$$A_{Ba} = \alpha \quad (17)$$

$$A_{Bc} = \beta \quad (18)$$

where

$$\alpha = \frac{(C_{11} - C_{12})(C_{33} - C_{13}) - (C_{23} - C_{13})(C_{11} - C_{13})}{(C_{33} - C_{13})(C_{22} - C_{12}) - (C_{13} - C_{23})(C_{12} - C_{23})} \quad (19)$$

$$\beta = \frac{(C_{22} - C_{12})(C_{11} - C_{13}) - (C_{11} - C_{12})(C_{23} - C_{12})}{(C_{22} - C_{12})(C_{33} - C_{13}) - (C_{12} - C_{23})(C_{13} - C_{23})} \quad (20)$$

For these parameters, the value of 1 indicates elastic isotropy, and similarly any deviation from 1 corresponds to a degree of elastic anisotropy. From the calculation result of the elastic constant, it can be observed that the bulk modulus anisotropy index $A_{Ba} = A_{Bc} = 1$. Therefore, the calculations show once again that Ni₃Al exhibit isotropic bulk modulus.

Table 4. The calculated anisotropic index of Ni₃Al.

Anisotropic Index	A^U	A_B	A_G	A_1	A_2	A_3	A_{Ba}	A_{Bc}
Value	1.670	0.000	0.145	3.093	3.093	3.093	1.000	1.000

To further investigate the anisotropic features of Ni₃Al crystal, the three-dimensional surface representation of the elastic anisotropy of the crystal was performed. The direction dependences of the Bulk modulus and Young's modulus of cubic crystal system are shown in the following Equations (21) and (22), respectively [49]

$$\frac{1}{B} = (S_{11} + 2S_{12}) \left(l_1^2 + l_2^2 + l_3^2 \right) \quad (21)$$

$$\frac{1}{E} = S_{11} - 2 \left(S_{11} - S_{12} - \frac{S_{44}}{2} \right) \left(l_1^2 l_2^2 + l_2^2 l_3^2 + l_1^2 l_3^2 \right) \quad (22)$$

where 11, 12, and 13 denote the direction cosines with respect to the a, b, and c directions of the lattice. As mentioned before, for Ni₃Al, the bulk modulus B has no anisotropy and its spatial three-dimensional (3D) surface representation is spherical, as shown in Figure 2a. For Young's modulus, its 3D surface representation is shown in Figure 2b, which exhibits obvious anisotropy.

In order to better understand the anisotropic characteristics, the Young's modulus of the Ni₃Al single crystal in the normal direction of the three low-index crystal planes {100}, {110} and {111} were calculated. The formula can be written as follows [50]

$$\frac{1}{E_{hkl}} = S_{11} - 2S_0 \frac{(hk)^2 + (hl)^2 + (lk)^2}{(h^2 + k^2 + l^2)^2} \quad (23)$$

where

$$S_0 = S_{11} - S_{12} - \frac{1}{2} S_{44} \quad (24)$$

The corresponding calculation results are listed in Table 5. The maximum and minimum values of Young's moduli are 304.241 GPa and 112.094 GPa along the normal direction of {111} and {100} planes, respectively, which are consistent with the results shown in Figure 2b.

In addition, the three-dimensional surface of the shear modulus of Ni₃Al can be expressed by Equation (25) [51]:

$$\frac{1}{G} = (S_{44} + 4S_0 J) \quad (25)$$

where

$$J = \sin^2 \theta \cdot \cos^2 \theta + 0.125 \cdot \sin^4 \theta (1 - \cos 4\theta) \quad (26)$$

wherein θ and ϕ are Euler angles, as shown in Figure 3. Figure 2c shows the shear moduli of Ni₃Al along different orientations. Clearly, shear modulus anisotropy can be deduced, with the maximum and minimum values are 123.831 GPa along <001> directions and 51.696 GPa along <111> directions, respectively. Generally, the direction dependence of shear modulus is opposite to that of Young's modulus.

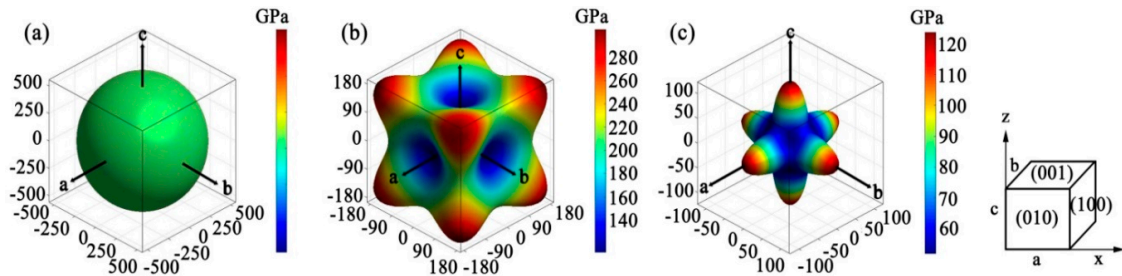


Figure 2. Directional dependence of bulk modulus (a), Young's modulus (b) and shear modulus (c).

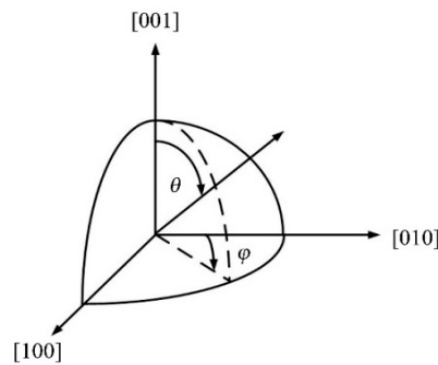


Figure 3. Coordinates system and Eulerian angles.

Table 5. Values of Young's moduli along normal directions of planes {100}, {110} and {111}.

Planes	{100}	{110}	{111}
E_{hkl} , GPa	112.094	212.973	304.241

Further, anisotropies of Poisson's ratios were also investigated by calculating the values along three lower-index planes. As for cubic crystal, the Poisson's ratio ν along arbitrary directions in (hkl) planes can be expressed as [50].

$$\nu(hkl, \theta) = \left\{ S_{12} + \frac{S_0}{h^2+k^2+l^2} \left[\left(\frac{h^2l}{\sqrt{h^2+k^2}\sqrt{h^2+k^2+l^2}} \cos \theta - \frac{hk}{\sqrt{h^2+k^2}} \sin \theta \right)^2 + \left(\frac{k^2l}{\sqrt{h^2+k^2}\sqrt{h^2+k^2+l^2}} \times \cos \theta + \frac{hk}{\sqrt{h^2+k^2}} \sin \theta \right)^2 + \left(\frac{l\sqrt{h^2+k^2}}{\sqrt{h^2+k^2+l^2}} \cos \theta \right)^2 \right] \right\} / \left[-S_{11} + 2S_0 \frac{(hk)^2+(hl)^2+(lk)^2}{(h^2+k^2+l^2)^2} \right] \quad (27)$$

Variations of Poisson's ratios in two low index planes, (100) and (111) are shown in Figure 4a,b, where Poisson's ratios are 0.400 and 0.228 correspondently, with no direction dependences. However, ν in (110) plane exhibits conspicuous anisotropic behaviour, see Figure 4c, where the maximum value 0.76 appears along [001] and [00 $\bar{1}$] directions, while the minimum value is -0.14 along the orientations of [$\bar{1}$ 10] and [1 $\bar{1}$ 0]. Poisson's ratios along two orthogonal symmetric directions in three low index planes of Ni₃Al are listed in Table 6.

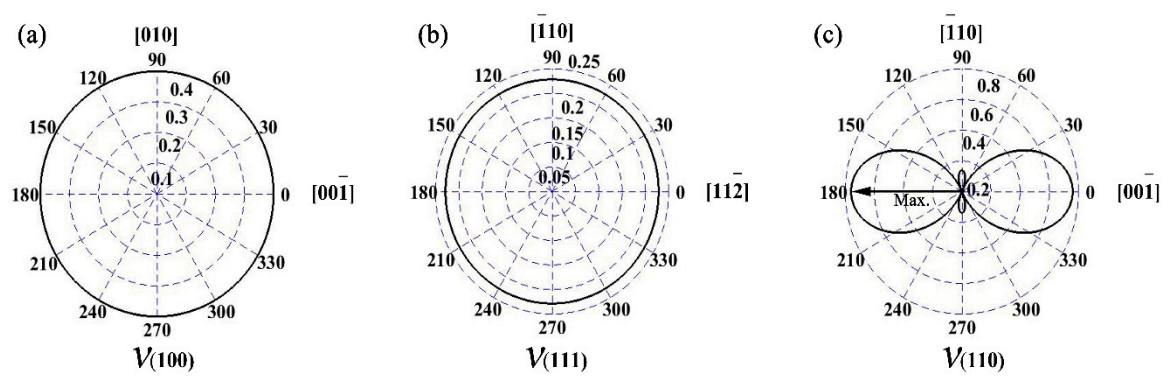


Figure 4. Curves of direction dependences of Poisson's ratios for typical low index planes (100) (a), (111) (b) and (110) (c).

Table 6. Poisson's ratios along two orthogonal symmetric directions in three low index planes of Ni₃Al.

Plane	(100)		(110)		(111)	
Direction	[010]	[00 $\bar{1}$]	$\bar{[110]}$	[00 $\bar{1}$]	$\bar{[110]}$	[11 $\bar{2}$]
Poisson's ratio	0.400	0.400	−0.140	0.760	0.228	0.228

3.4. Thermodynamic Properties

As a fundamental parameter, the Debye temperature (θ_D) correlates with many physical properties of solids, such as specific heat, elastic constant and melting temperature [48]. One of the standard methods to calculate the Debye temperature can be estimated from the averaged sound velocity (v_m) by Equation (28) [52]

$$\theta_D = \frac{\hbar}{k_B} \left(\frac{3nN_A\rho}{4\pi M} \right)^{1/3} v_m \quad (28)$$

where \hbar is Planck's constant, k_B is Boltzmann's constant, N_A is Avogadro's number, ρ is the density, M is the molecular weight and n is the number of atoms in a molecule. The average wave velocity v_m is approximately given by [52]

$$v_m = \left[\frac{1}{3} \left(\frac{1}{v_l^3} + \frac{2}{v_t^3} \right) \right]^{-1/3} \quad (29)$$

$$v_l = \left(\frac{3B + 4G}{3\rho} \right)^{1/2} \quad (30)$$

$$v_t = \left(\frac{G}{\rho} \right)^{1/2} \quad (31)$$

among them, v_l and v_t are the longitudinal and transverse elastic wave velocities of the polycrystalline material that are determined by bulk modulus (B) and shear modulus (G). Based on the calculated elastic properties, the results are listed in Table 7 accordingly. It can be pointed out that the calculated Debye temperature is 475.734 K, which is similar to the experimental value 460 K [53], approving the accuracy of the calculation results in this study.

Table 7. The calculated thermodynamic properties of Ni₃Al at zero pressure.

Property	ρ , g/cm ³	v_t , m/s	v_l , m/s	v_m , m/s	θ_D , K
Value	7.371	3270.809	6292.559	3660.396	475.734

4. Conclusions

First principles density functional calculations were applied to extensively explore the mechanical properties and elastic anisotropies of cubic Ni₃Al single crystal. The calculated lattice constants are found to be in good agreement with experimental data, revealing the effectiveness of the proposed theoretical models. The calculated bulk modulus, Young's modulus, shear modulus and Poisson's ratio of polycrystalline Ni₃Al are 186.724 GPa, 207.378 GPa, 78.857 GPa and 0.315 respectively, which are consistent with experimental values. The calculated *B/G* ratio implies that Ni₃Al single crystal is a ductile material. Anisotropies of mechanical properties were studied by computing varied anisotropic indices and directional dependences of bulk modulus, Young's modulus, shear modulus and Poisson's ratio of monocrystalline Ni₃Al. There is no anisotropy for bulk modulus of Ni₃Al, while the Young's modulus exhibits evident anisotropy, with the largest value 304.241 GPa along the normals of {111} planes and the minimum value 112.094 GPa along the {100} planes normals. In addition, the direction dependence of shear modulus is opposite to that of Young's modulus, and the shear modulus takes the maximum value of 123.831 GPa in the <100> directions while the minimum value 51.696 GPa is assigned along the <111> directions. Poisson's ratio shows isotropy on the (100) and (111) planes respectively. In (110) plane, however, Poisson's ratio depends strongly on the direction, with the minimum value of only 0.140, while the maximum value is 0.760. Furthermore, the calculated Debye temperature based on the calculated elastic constants is 475.734 K, which is close to the experimental value 460K; thus the accuracy of the calculation results is further approved.

Author Contributions: H.Q. and F.L. conceived and designed the research; H.Q., X.L., F.L. and Q.L. performed the first principles calculation; X.L. wrote the manuscript; Y.Y. and Z.D. reviewed and edited the manuscript. All authors read and approved the final manuscript.

Funding: This research was funded by the GDAS' Project of Science and Technology Development (No. 2018GDASCX-1005), Key Program for International Cooperation of Science and Technology (No. 2015DFR50310), National Natural Science Foundation of China (No. 51505095) and Science and Technology Plan Project Public Welfare Fund and Ability Construction Project of Guangdong province (No. 2017A070701026).

Conflicts of Interest: The authors declare no conflict of interest.

References

1. Wen, Z.; Zhao, Y.; Hou, H.; Tian, J.; Han, P. First-principles study of Ni-Al intermetallic compounds under various temperature and pressure. *Superlattices Microstruct.* **2017**, *103*, 9–18. [[CrossRef](#)]
2. Wen, M.; Wang, C.Y. Transition-metal alloying of γ' -Ni₃Al: Effects on the ideal uniaxial compressive strength from first-principles calculations. *Phys. Rev. B* **2018**, *97*, 024101. [[CrossRef](#)]
3. Goiri, J.G.; Ven, A.V.D. Phase and structural stability in Ni-Al systems from first principles. *Phys. Rev. B* **2016**, *94*, 094111. [[CrossRef](#)]
4. Jiang, L.; Li, S.; Han, Y. Rotating bending fatigue property of the Ni₃Al-based single crystal superalloy IC6SX at 900 °C. *Mater. Sci. Eng.* **2017**, *182*, 012058.
5. Jozwik, P.; Polkowski, W.; Bojar, Z. Applications of Ni₃Al based intermetallic alloys γ current stage and potential perceptivities. *Materials* **2015**, *8*, 2537–2568. [[CrossRef](#)]
6. Hou, H.; Wen, Z.; Zhao, Y.; Fu, L.; Wang, N.; Han, P. First-principles investigations on structural, elastic, thermodynamic and electronic properties of Ni₃X (X=Al, Ga and Ge) under pressure. *Intermetallics* **2014**, *44*, 110–115. [[CrossRef](#)]
7. Chen, D.; Luo, F.; Lou, X.; Qing, Y.; Zhou, W.; Zhu, D. Comparison of thermal insulation capability between conventional and nanostructured plasma sprayed ysz coating on Ni₃Al substrates. *Ceram. Int.* **2016**, *43*, 4324–4329. [[CrossRef](#)]
8. Pearson, W.B.; Raynor, G.V. *A Handbook of Lattice Spacings and Structures of Metals and Alloys*; Elsevier: Amsterdam, The Netherlands, 2013.
9. Yasuda, H.; Takasugi, T.; Koiwa, M. Elasticity of Ni-based L₁₂-type intermetallic compounds. *Acta Metall.* **1992**, *40*, 381–387. [[CrossRef](#)]
10. Qin, H.; Luan, X.; Feng, C. Mechanical, thermodynamic and electronic properties of wurtzite and zinc-blende gan crystals. *Materials* **2017**, *10*, 1419. [[CrossRef](#)] [[PubMed](#)]

11. Liu, D.; Zhu, X.; Qin, J.; Wang, A.; Duan, J.; Gu, T. First-principles study of chemical and topological short-range orders in the Mg–Si liquid alloys. *Metals* **2016**, *6*, 78. [[CrossRef](#)]
12. Huang, H.; Zhang, C.; Liu, J.; Li, Y.; Fang, X.; Li, J.; Han, P. First-principles study on the structural stability and segregation behavior of γ -Fe/Cr₂N interface with alloying additives M (M = Mn, V, Ti, Mo, and Ni). *Metals* **2016**, *6*, 156. [[CrossRef](#)]
13. Li, X.; Xia, C.; Wang, M.; Wu, Y.; Chen, D. First-principles investigation of structural, electronic and elastic properties of HfX (X = Os, Ir and Pt) compounds. *Metals* **2017**, *7*, 317. [[CrossRef](#)]
14. Liu, Y.; Huang, Y.; Xiao, Z.; Reng, X. Study of adsorption of hydrogen on Al, Cu, Mg, Ti surfaces in al alloy melt via first principles calculation. *Metals* **2017**, *7*, 21. [[CrossRef](#)]
15. Kim, D.E.; Shang, S.L.; Liu, Z.K. Effects of alloying elements on elastic properties of NiAl by first-principles calculations. *Intermetallics* **2010**, *18*, 1163–1171. [[CrossRef](#)]
16. Huang, M.L. First-principles studies of effects of interstitial boron and carbon on the structural, elastic, and electronic properties of Ni solution and Ni₃Al intermetallics. *Chin. Phys. B* **2016**, *25*, 107104. [[CrossRef](#)]
17. Ai, C.; Li, S.; Zhao, X.; Zhou, J.; Guo, Y.; Sun, Z.; Song, X.; Gong, S. Influence of solidification history on precipitation behavior of TCP phase in a completely heat-treated Ni₃Al based single crystal superalloy during thermal exposure. *J. Alloy Compd.* **2017**, *722*, 740–745. [[CrossRef](#)]
18. Jiang, L.; Li, S.; Han, Y. Research on the creep mechanism of a Ni₃Al-based single crystal superalloy IC6SX under 980 °C/205MPa. *Mater. Sci. Eng.* **2017**, *182*, 012059.
19. Jiang, L.W.; Wu, M.L.; Li, S.S.; Han, Y.F. Rotating bending fatigue behaviour of a Ni₃Al-based single crystal alloy IC6SX at 760 °C. *Mater. Res. Innov.* **2015**, *19*, S163–S169. [[CrossRef](#)]
20. Zhang, J.M.; Zhang, Y.; Xu, K.W. Dependence of stresses and strain energies on grain orientations in FCC metal films. *J. Cryst. Growth* **2005**, *285*, 427–435. [[CrossRef](#)]
21. Choi, J.H.; Kang, S.Y.; Dong, N.L. Relationship between deposition and recrystallization textures of copper and chromium electrodeposits. *J. Mater. Sci.* **2000**, *35*, 4055–4066. [[CrossRef](#)]
22. Mohan Rao, P.V.; Suryanarayana, S.V.; Satyanarayana Murthy, K.; Nagender Naidu, S.V. The high-temperature thermal expansion of Ni₃Al measured by X-ray diffraction and dilation methods. *J. Phys. Condens. Matter* **1989**, *1*, 5357.
23. Lindan, P.J.D.; Probert, M.J.; Segall, M.D.; Pickard, C.J.; Hasnip, P.; Clark, S.J.; Payne, M.C. First-principles simulation. *J. Phys. Condens. Matter* **2002**, *14*, 2717–2744.
24. Monkhorst, H.J. Special points for brillouin-zone integrations. *Phys. Rev. B Condens. Matter* **1976**, *16*, 1748–1749. [[CrossRef](#)]
25. Perdew, J.P.; Burke, K.; Ernzerhof, M. Generalized gradient approximation made simple. *Phys. Rev. Lett.* **1996**, *77*, 3865. [[CrossRef](#)] [[PubMed](#)]
26. Kohn, W.; Sham, L.J. Self-consistent equations including exchange and correlation effects. *Phys. Rev.* **1965**, *140*, A1133–A1138. [[CrossRef](#)]
27. Martin, R.; Nagathil, A. Stability investigation and thermal behavior of a hypothetical silicon nanotube. *J. Mol. Struct. Theochem.* **2001**, *539*, 101–106.
28. Hammer, B. Improved adsorption energetics within density-functional theory using revised Perdew-Burke-Ernzerhof functionals. *Phys. Rev. B* **1999**, *59*, 7413–7421. [[CrossRef](#)]
29. Francis, G.P.; Payne, M.C. Finite basis set corrections to total energy pseudopotential calculations. *J. Phys. Condens. Matter* **1999**, *2*, 4395. [[CrossRef](#)]
30. Kumar, S.; Jung, J.P. Mechanical and electronic properties of Ag₃Sn intermetallic compound in lead free solders using ab initio atomistic calculation. *Mater. Sci. Eng. B* **2013**, *178*, 10–21. [[CrossRef](#)]
31. Lee, N.T.S.; Tan, V.B.C.; Lim, K.M. Structural and mechanical properties of Sn-based intermetallics from ab initio calculations. *Appl. Phys. Lett.* **2006**, *89*, 353–489. [[CrossRef](#)]
32. Chen, J.; Lai, Y.S. Towards elastic anisotropy and strain-induced void formation in Cu-Sn crystalline phases. *Microelectron. Reliab.* **2009**, *49*, 264–268. [[CrossRef](#)]
33. Nguyen-Manh, D.; Pettifor, D.G. Electronic structure, phase stability and elastic moduli of ab transition metal aluminides. *Intermetallics* **1999**, *7*, 1095–1106. [[CrossRef](#)]
34. Chen, W.H.; Yu, C.F.; Cheng, H.C.; Lu, S.T. Crystal size and direction dependence of the elastic properties of Cu₃Sn through molecular dynamics simulation and nanoindentation testing. *Microelectron. Reliab.* **2012**, *52*, 1699–1710. [[CrossRef](#)]

35. Fatmi, M.; Ghebouli, M.A.; Ghebouli, B.; Chihi, T.; Boucetta, S.; Heiba, Z.K. Study of structural, elastic, electronic, optical and thermal properties of Ni₃Al. *Rom. J. Phys.* **2011**, *56*, 935–951.
36. Zhao, W.; Sun, Z.; Gong, S. Synergistic effect of co-alloying elements on site preferences and elastic properties of Ni₃Al: A first-principles study. *Intermetallics* **2015**, *65*, 75–80. [[CrossRef](#)]
37. Kayser, F.X.; Stassis, C. The elastic constants of Ni₃Al at 0 and 23.5 °C. *Phys. Status Solidi* **2010**, *64*, 335–342. [[CrossRef](#)]
38. Nye, J.F.; Lindsay, R.B. *Physical Properties of Crystals: Their Representation by Tensors and Matrices*; Oxford University Press: Oxford, UK, 1984.
39. Verma, J.K.D.; Nag, B.D. On the elastic moduli of a crystal and voigt and reuss relations. *J. Phys. Soc. Jpn.* **2007**, *20*, 635–636. [[CrossRef](#)]
40. Hill, R. The elastic behaviour of a crystalline aggregate. *Proc. Phys. Soc.* **2002**, *65*, 349–354. [[CrossRef](#)]
41. Prikhodko, S.V.; Yang, H.; Ardell, A.J.; Carnes, J.D. Temperature and composition dependence of the elastic constants of Ni₃Al. *Metall. Mater. Trans. A* **1999**, *30*, 2403–2408. [[CrossRef](#)]
42. Pugh, S.F. XCII. Relations between the elastic moduli and the plastic properties of polycrystalline pure metals. *Philos. Mag.* **2009**, *45*, 823–843. [[CrossRef](#)]
43. Aoki, K.; Izumi, O. On the ductility of the intermetallic compound Ni₃Al. *Mater. Trans.* **2007**, *19*, 203–210.
44. Liu, Z.T.Y.; Gall, D.; Khare, S.V. Electronic and bonding analysis of hardness in pyrite-type transition-metal pernitrides. *Phys. Rev. B* **2014**, *90*, 134102. [[CrossRef](#)]
45. Tian, Y.; Xu, B.; Zhao, Z. Microscopic theory of hardness and design of novel superhard crystals. *Int. J. Refract. Met. Hard Mater.* **2012**, *33*, 93–106. [[CrossRef](#)]
46. Ranganathan, S.I.; Ostoja-Starzewski, M. Universal elastic anisotropy index. *Phys. Rev. Lett.* **2008**, *101*, 055504. [[CrossRef](#)] [[PubMed](#)]
47. Vahldiek, F.W.; Mersol, S.A. *Anisotropy in Single-Crystal Refractory Compounds*; Springer: New York, NY, USA, 1968.
48. Ravindran, P.; Fast, L.; Korzhavyi, P.A.; Johansson, B.; Wills, J.; Eriksson, O. Density functional theory for calculation of elastic properties of orthorhombic crystals: Application to TiSi₂. *J. Appl. Phys.* **1998**, *84*, 4891–4904. [[CrossRef](#)]
49. Huang, B.; Duan, Y.H.; Hu, W.C.; Sun, Y.; Chen, S. Structural, anisotropic elastic and thermal properties of Mb (M=Ti, Zr and Hf) monoborides. *Ceram. Int.* **2015**, *41*, 6831–6843. [[CrossRef](#)]
50. Zhang, J.M.; Zhang, Y.; Xu, K.W.; Ji, V. Young's modulus surface and poisson's ratio curve for cubic metals. *J. Phys. Chem. Solids* **2007**, *68*, 503–510. [[CrossRef](#)]
51. Wu, Q.; Li, S. Alloying element additions to Ni₃Al: Site preferences and effects on elastic properties from first-principles calculations. *Comput. Mater. Sci.* **2012**, *53*, 436–443. [[CrossRef](#)]
52. Anderson, O.L. A simplified method for calculating the debye temperature from elastic constants. *J. Phys. Chem. Solids* **1963**, *24*, 909–917. [[CrossRef](#)]
53. Ho, J.C.; Liang, R.C.; Dandekar, D.P. Low temperature heat capacities of Ni₃Al. *J. Appl. Phys.* **1986**, *59*, 1397–1398. [[CrossRef](#)]

